



Original software publication

Open source vector field topology

Roxana Bujack^{a,*}, Karen Tsai^a, Steven K. Morley^a, Etienne Bresciani^{b,c}^a Los Alamos National Laboratory, United States of America^b Korea Institute of Science and Technology (KIST), Seoul, South Korea^c Center for Advanced Studies in Arid Zones (CEAZA), La Serena, Chile

ARTICLE INFO

Article history:

Received 1 February 2021

Received in revised form 20 July 2021

Accepted 27 July 2021

Keywords:

Vector field

Topology

Critical point

Separatrix

ABSTRACT

A myriad of physical phenomena, such as fluid flows, magnetic fields, and population dynamics are described by vector fields. More often than not, vector fields are complex and their analysis is challenging.

Vector field topology is a powerful analysis technique that consists in identifying the most essential structure of a vector field. Its topological features include critical points and separatrices, which segment the domain into regions of coherent flow behavior, provide a sparse and semantically meaningful representation of the underlying data.

However, a broad adoption of this formidable technique has been hampered by the lack of open source software implementing it. The Visualization Toolkit (VTK) now contains the filter `vtkVectorFieldTopology` that extracts the topological skeleton of 2D and 3D vector fields. This paper describes our implementation and demonstrates its broad applicability with two real-world examples from hydrology and space physics.

Published by Elsevier B.V. This is an open access article under the CC BY-NC-ND license (<http://creativecommons.org/licenses/by-nc-nd/4.0/>).

Code metadata

Current code version	9.0.1
Permanent link to code/repository used for this code version	https://github.com/ElsevierSoftwareX/SOFTX-D-21-00026
Code Ocean compute capsule	none
Legal Code License	BSD
Code versioning system used	git
Software code languages, tools, and services used	C, C++, Python
Compilation requirements, operating environments & dependencies	Cross-platform
If available Link to developer documentation/manual	https://vtk.org/doc/nightly/html/classvtkVectorFieldTopology.html
Support email for questions	bujack@lanl.gov

1. Motivation and significance

Vector field analysis is critically important for many scientific applications, such as aeronautic engineering, material sciences, environmental sciences, and space sciences. The vector fields involved in these applications are typically complex, making it challenging for humans to visualize and describe them in a comprehensive manner. Vector field topology is a powerful analysis technique that addresses this challenge through the identification of the topological features of vector fields [1–5].

The topological features of a vector field comprise a finite set of elements or properties that reveal the most essential structure of the vector field. Being finite, this set of elements is typically much easier to visualize and describe than the complete vector field. Identifying these elements also enables the automatic qualitative and quantitative analysis of vector fields by revealing the number of critical points and the numbers and sizes of regions of coherent behavior. Tracked over time or over a change in system parameter, such information provides insight on changes of the overall behavior of the system.

Our code computes the topological skeleton of 2D and 3D vector fields. Essentially, the topological skeleton of a vector field is a sparse set of trajectories that reveals the topological structure of the flow defined by the vector field. More specifically, the

* Corresponding author.

E-mail address: bujack@lanl.gov (Roxana Bujack).

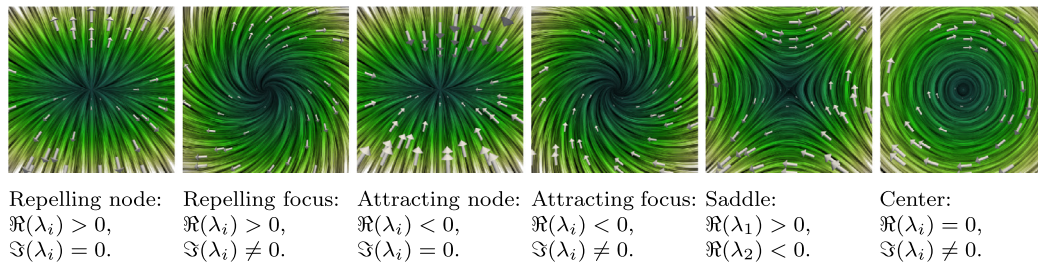


Fig. 1. The different types of nondegenerate 2D critical points visualized with line integral convolution (LIC) [6] and arrow glyphs. Here the presence of the subscript i means all $i \in (1, 2, 3)$, and the order of the eigenvalues does not matter.

topological skeleton of a d -dimensional vector field $v : \mathbb{R}^d \rightarrow \mathbb{R}^d$ consists of its separatrices, which are solution trajectories (*streamlines* in the language of fluid mechanics) that differ from their neighbors in their origin or destination [7,8]. Thus, separatrices are boundaries between regions of radically different behavior. Separatrices include critical points (i.e., the points at which $v(x) = 0$) and associated invariant manifolds (i.e., lines or surfaces comprising trajectories that have a critical point as origin or destination). Other, less obvious types of separatrices exist (e.g., closed trajectories, boundary switches [5]), but these are not computed in the current version of the code (this may be added in future releases). A significant amount of research has been done on topology-based visualization techniques [9–12] building on the foundation of critical points and separatrices.

To the best of our knowledge, our code is the first open source implementation enabling computation of the topological skeleton of vector fields.

2. Software description

2.1. Software architecture

We developed a new filter (*vtkVectorFieldTopology*) in the Visualization Toolkit (VTK) [13,14]. VTK is a popular open source software system for data processing, analysis, and visualization. It is object-oriented and provides many useful data objects and ‘filters’ to create objects or operate on them. Its pipeline architecture allows for setting up elaborate workflows by connecting and combining several filters. VTK is written in C++ ensuring high performance, and a hybrid wrapper facility allows for generating language bindings to Python, Java, and Tcl for easy access. Thus, by adopting the VTK framework, our code can be easily combined with other functionalities available in VTK, and it is accessible through several programming languages.

2.2. Software functionalities

The new filter takes a 2D or 3D *vtkDataSet* object as input and it computes the topological skeleton of a user-specified vector field stored as part of the point data. In 2D, the output consists of two *vtkPolyData* objects. The first one contains the critical points, and the second one contains the 1D separatrices (i.e., lines). In 3D, an optional third *vtkPolyData* object is produced that contains the 2D separatrices (i.e., surfaces). Relevant information is also added to the point data of these objects, as explained later.

The algorithm starts by finding the critical points $x \in \mathbb{R}^d : v(x) = 0$. It does so analytically after triangulation (tetrahedralization) of the data and based on a linear interpolation inside the cells [2,5]. The critical points are then classified based on the eigenvalues of the Jacobian $\nabla v \in \mathbb{R}^{d \times d}$ of the vector field [8]. The $d \times d$ matrix ∇v is also evaluated analytically inside the cells, and its eigenvalues $\{\lambda_i, i \in (1, 2, \dots, d)\}$ are computed using the Eigen library [15].

In 2D, the most common (i.e., nondegenerate) types of critical points are sources, sinks, saddles, and centers, summarized in Fig. 1. Sources and sinks can be further divided into two sub-categories based on the imaginary part of the eigenvalues: if it is zero, the trajectories approach the critical point along specific directions, whereas if it is nonzero, the trajectories approach the critical point rotating around it indefinitely. The four corresponding cases are called repelling node, repelling focus, attracting node, and attracting focus. Four 1D separatrices originate or terminate at a saddle (two originate and two terminate). These separatrices are computed by placing four seeds at a small user-defined offset of the saddle in the direction of the eigenvectors of ∇v , which give the directions along which the separatrices approach the saddle. The trajectories from these seeds – the separatrices – are integrated using the filter *vtkStreamTracer*, which implements streamline integration through a choice of Runge–Kutta methods.

In 3D, the most common (i.e., nondegenerate) types of critical points are sources, sinks, repelling saddles, and attracting saddles, visualized in Fig. 2. Each of these types may imply a rotating pattern in a certain plane depending on the presence of eigenvalues with nonzero imaginary part. This gives rise to the eight cases shown in the figure. A 2D separatrix and two 1D separatrices originate or terminate at a saddle (if the 2D separatrix originates at the saddle, then the 1D separatrices terminate at the saddle, and vice-versa). The directions along which the separatrices approach the saddle are given by the eigenvectors of ∇v . The 1D separatrices are computed by placing two seeds at a small user-defined offset of the saddle in the direction of the eigenvectors of ∇v corresponding to the eigenvalue whose sign appears only once. The trajectories from these seeds are integrated as explained above. The 2D separatrix is computed by placing eight seeds at a small user-defined offset of the saddle in the plane spanned by the eigenvectors of ∇v corresponding to the eigenvalues whose signs appear twice. These seeds are the base for integrating a surface – the separatrix – using the filter *vtkStreamSurface*, which was developed as part of this project. This filter iteratively integrates trajectories and their connections into a triangulated surface one step at a time, reinserting additional streamlines if neighboring ones diverge too far from each other as suggested by Hultquist [16].

The most important input parameters are the distance in which the separatrices are seeded away from the saddles and the parameters that are handed off to the streamline and streamsurface integrators, like step sizes and maximum number of steps. All are described in the VTK documentation. The output object of type *vtkPolyData* containing the critical points stores information on the type and sub-type (i.e., whether a rotating pattern exists or not) of the critical points as well as the matrix ∇v . Furthermore, the output objects containing the separatrices store the integration time along the computed trajectories.

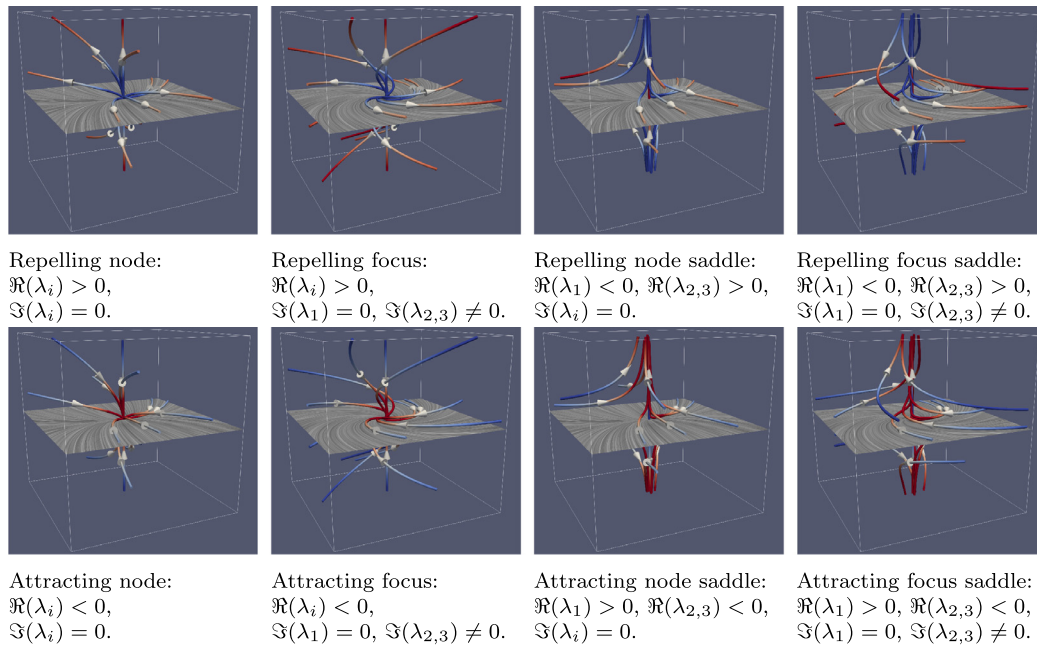


Fig. 2. The different types of nondegenerate 3D critical points visualized with streamlines color coded in red/blue for forward/backward integration and LIC in the plane of the common sign. Here the presence of the subscript i means all $i \in (1, 2, 3)$, and the order of the eigenvalues does not matter.

3. Illustrative examples

3.1. Groundwater flow

Water that infiltrates into the ground becomes groundwater. Groundwater typically flows through several geological layers before reappearing on the ground surface in the form of springs, river baseflow, or wetlands. It is both an essential part of the water cycle and a major resource of water for humans. Thus, characterizing groundwater flow is critical to understand and manage freshwater ecosystems and water resources.

To illustrate the new VTK filter in this context, we performed 2D and 3D simulations of groundwater flow around an extraction–injection well pair embedded in a regional flow field. This type of system is commonly used in various applications including aquifer storage and recovery [17], geothermal energy systems [18], and in-situ bioremediation of contaminated groundwater [19]. The critical points and separatrices as extracted by our algorithm from the simulations are visualized in Fig. 3. The 2D simulation (left) assumes purely horizontal flow, whereas the 3D simulation (right) assumes that the injection and extraction wells are modeled as points located midway between the top and the bottom of the aquifer. In both cases, the wells are aligned at an angle to the direction of the regional flow field, and the flow is simulated in steady state. The simulations were performed with the MODFLOW-2005 code [20].

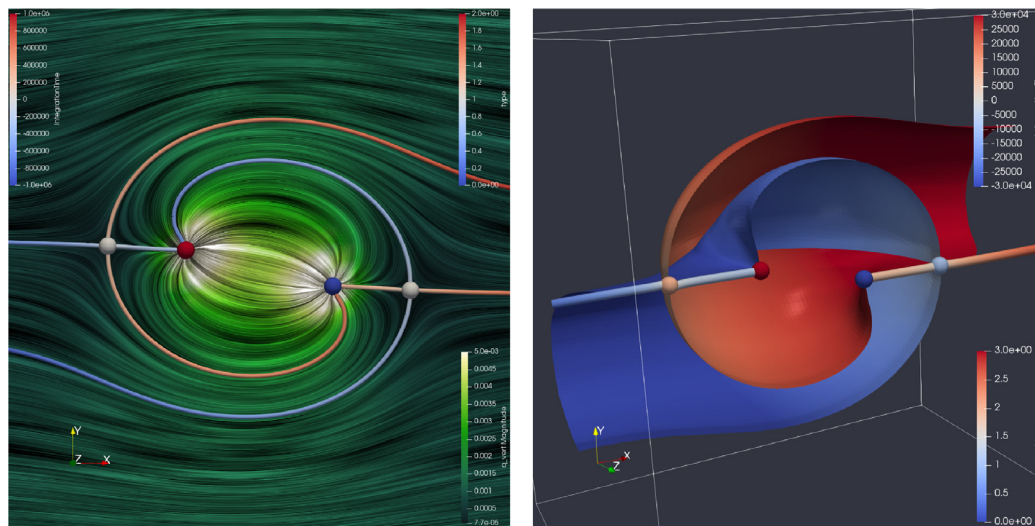
There are three distinct flow zones that are important to delineate in this system: a capture zone in which regional groundwater flows towards the extraction well, a transfer zone in which injected water flows towards the extraction well, and a release zone in which injected water is lost to the regional system [21]. Fig. 3 demonstrates that the topological skeleton computed using the new filter effectively delineates these three zones and separates them from the background flow in 2D as well as in 3D. Note that the extraction and injection wells are detected as critical points even if in reality, velocity is not zero at these points: instead, velocity is maximum at the wells. This results from the interpolation inside a cell when the flow is inward on all sides of the cell (or outward on all sides of the cell). Physically, these points are sources and sinks, and, as such, it is a good thing that they are identified by the algorithm.

3.2. Magnetospheric dynamics

Earth’s magnetosphere is the region of near-Earth space dominated by the terrestrial, rather than the solar, magnetic field. The primary mechanism for driving magnetospheric dynamics is energy transfer through magnetic reconnection on the day side [22,23] and subsequent release on the night side through magnetic reconnection [24,25]. Identifying the magnetic separatrices and critical points in global simulations is important for understanding energy transfer in the magnetosphere [26].

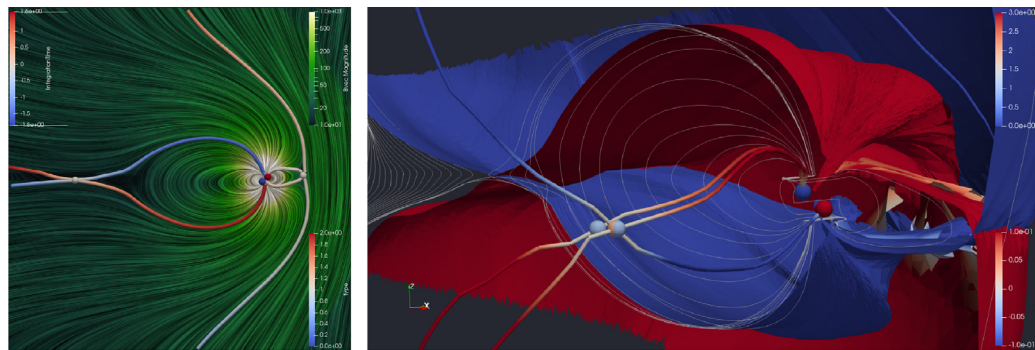
Following [26] we use the Space Weather Modeling Framework (SWMF; [27]) to demonstrate the identification of the vector field topology using VTK. SWMF couples together component models to simulate a variety of space physics domains in a self-consistent manner, and here we use the same set of component models as the operational version in use at the National Oceanic and Atmospheric Administration (NOAA) Space Weather Prediction Center [28]. The core component is the Block-Adaptive Tree Solarwind Roe-type Upwind Scheme (BATS-R-US) [29], which solves the magnetohydrodynamic equations. Among other state variables, BATS-R-US calculates the evolution of the vector magnetic field, \vec{B} . In this example we examine the output from the BATS-R-US model using the “high-resolution” (1.94M cells, 7 refine levels) configuration from [30].

Fig. 4 shows the application of the vector topology filters to a snapshot in time from the SWMF simulation of a severe geomagnetic storm [31] on 12 August 2000 [32]. Fig. 4a shows the vector topology in a 2D slice in the X–Z plane of the simulation; that is, this represents a cut-through of the magnetosphere seen from the side of the Earth with the Sun to the right (+ve X direction). In two dimensions, the configuration is exactly that predicted by Dungey’s “open magnetosphere” model [22]. It identifies a source and a sink at the Earth’s poles and 2 saddles, whose separatrices separate the domain into 6 regions of coherent vector field behavior: 2 in the center with origin and destination being the Earth’s poles (“closed”), 2 on top and below being connected to one pole without returning to the other (“open”), and 2 left and right not connected to either pole (“interplanetary”). Fig. 4b illustrates the topology in three dimensions, which reveals that the 2 separate



2D topology on top of line integral convolution (LIC) [15]. Critical points color coded red: repelling, blue: attracting, white: saddle. 3D topology cutoff along $Z = 0$ plane. Critical points color coded; red: repelling, blue: attracting, light pink: 2 saddle, light blue: 1 saddle.

Fig. 3. Vector field topology of groundwater flow around an extraction–injection well pair embedded in a regional flow field. The integration time along the separatrices is encoded in color, red: forward, blue: backward in time.



2D topology on top of LIC. Critical points color coded red: repelling, blue: attracting, white: saddle. 3D topology cutoff along the $Y = 0$ plane to allow view onto the behavior next to the Earth. Critical points color coded; red: repelling, blue: attracting, light pink: 2 saddle, light blue: 1 saddle.

Fig. 4. Vector field topology of a simulation of the magnetic field around the Earth in interaction with the Sun's. The integration time along the separatrices is encoded in color, red: forward, blue: backward in time.

regions of coherent vector field behavior connecting the Earth's poles from the 2D image is actually one connected component surrounding the Earth. The magnetic reconnection sites transferring flux between open and closed regions will then lie along the separatrix [26,33].

4. Impact

Despite vector field topology being a powerful analysis technique with a solid theoretical foundation, we feel that this technique has been underutilized by the scientific community at large. Being the first open source code to compute the topological skeleton of vector fields, this contribution has the potential to greatly increase the adoption of topology-based analysis techniques by scientists. VTK is widely used in scientific computing, computational geometry, and medical image analysis. It is the underlying library for many popular visualization tools (e.g., ParaView [34], VisIT [35]), making our code directly accessible to a large group

of users. As vector fields are ubiquitous in science, this code will foster scientific discoveries and benefit numerous applications in various disciplines.

Hydrogeology, for example, will greatly benefit from this tool. Critical points occur in many groundwater flow problems [36], and the separatrices associated to these points constitute water divides between regions connected to different recharge areas or different discharge areas [37]. Identifying, delineating and analyzing these different regions sheds light on groundwater–surface water interactions, the capture zone of pumping wells, and solute transport in groundwater flow systems [38–40]. Yet, until recently, this type of analysis has principally been conducted in simplistic configurations in 2D [41–43]. Our code will hence allow for tackling long-standing questions about the structure of groundwater flow in more realistic configurations. This will yield a better understanding of the water cycle and facilitate the development of effective water resources management strategies.

5. Conclusions

Many physical phenomena, like, the movement of material, gravitational, magnetic, or electric fields are described by vector fields. One of their most popular analysis techniques is vector field topology, because it breaks down even huge amounts of data into a compact, sparse, and easy to comprehend description with little information loss.

To the best of our knowledge, we have presented the first open source implementation that extracts the critical points and their associated streamlines segmenting a given vector field into its most basic components, which facilitates the analysis of complex vector fields. The algorithm works in 2D and 3D as well as on structured and unstructured data. It is integrated into VTK for broad accessibility by application scientists from all domains, and we have illustrated its utility by application to hydrological and space physics simulation data.

We hope our contribution will further research and development by enabling scientists and engineers working with vector fields to gain more insight into their data.

Declaration of competing interest

The authors declare that they have no known competing financial interests or personal relationships that could have appeared to influence the work reported in this paper.

Acknowledgments

We gratefully acknowledge the support of the U.S. Department of Energy through the LANL Laboratory Directed Research Development Program under project numbers 20190143ER and 20200065DR for this work. This work is published under LA-UR-20-29277. The authors also acknowledge support from the Korea Research Fellowship program funded by the Ministry of Science and ICT through the National Research Foundation of Korea (grant 2016H1D3A1908042). We would like to thank the Kitware team for their support with the integration of our filter into VTK, especially Mathieu Westphal, Charles Gueunet, Cory Quammen, and Will Schroeder.

References

- [1] Perry AE, Fairlie BD. Critical points in flow patterns. *Adv Geophys* 1974;18B:299–315. [http://dx.doi.org/10.1016/S0065-2687\(08\)60588-9](http://dx.doi.org/10.1016/S0065-2687(08)60588-9).
- [2] Helman J, Hesselink L. Representation and display of vector field topology in fluid flow data sets. *Computer* 1989;22(8):27–36. <http://dx.doi.org/10.1109/2.35197>.
- [3] Levit C, Lasinski T. A tool for visualizing the topology of three-dimensional vector fields. In: *Proc. visualization'91*. Citeseer; 1991, p. 33–40.
- [4] Asimov D. Notes on the topology of vector fields and flows. *Tech. Rep. RNR-93-003*, NASA Ames Research Center; 1993.
- [5] Theisel H, Rössl C, Weinkauff T. Topological representations of vector fields. In: *Shape analysis and structuring*. Springer; 2008, p. 215–40.
- [6] Cabral B, Leedom LC. Imaging vector fields using line integral convolution. In: *Proceedings of the 20th annual conference on computer graphics and interactive techniques*. SIGGRAPH '93, ACM; 1993, p. 263–70. <http://dx.doi.org/10.1145/166117.166151>.
- [7] Markus L. Global structure of ordinary differential equations in the plane. *Trans Amer Math Soc* 1954;76(1):127–48.
- [8] Perko L. *Differential equations and dynamical systems*, Vol. 7. Springer Science & Business Media; 2013.
- [9] Laramée RS, Hauser H, Zhao L, Post FH. Topology-based flow visualization, the state of the art. In: *Topology-based methods in visualization*. Springer; 2007, p. 1–19.
- [10] Pobitzer A, Peikert R, Fuchs R, Schindler B, Kuhn A, Theisel H, et al. The state of the art in topology-based visualization of unsteady flow. *Comput Graph Forum* 2011;30(6):1789–811. <http://dx.doi.org/10.1111/j.1467-8659.2011.01901.x>.
- [11] Heine C, Leitte H, Hlawitschka M, Iuricich F, De Florian L, Scheuermann A. A survey of topology-based methods in visualization. In: *Computer graphics forum*. Vol. 35. 35, (3); Wiley Online Library; 2016, p. 643–67.
- [12] Bujack R, Yan L, Hotz I, Garth C, Wang B. State of the art in time-dependent flow topology: Interpreting physical meaningfulness through mathematical properties. *Comput Graph Forum* 2020. <http://dx.doi.org/10.1111/cgf.14037>.
- [13] *The visualization toolkit user's guide*. Kitware, Inc.; 2003.
- [14] Schroeder WJ, Lorensen B, Martin K. *The visualization toolkit: An Object-oriented approach to 3D graphics*. Kitware; 2004.
- [15] Guennebaud G, Jacob B, et al. Eigen v3. 2010. <http://eigen.tuxfamily.org>.
- [16] Hultquist JP. Constructing stream surfaces in steady 3D vector fields. In: *Proceedings of the 3rd conference on visualization'92*. IEEE Computer Society Press; 1992, p. 171–8.
- [17] Dillon P. Future management of aquifer recharge. *Hydrogeol J* 2005;13(1):313–6. <http://dx.doi.org/10.1007/s10040-004-0413-6>.
- [18] Geothermal heat pump systems: Status review and comparison with other heating options. *Appl Energy* 2013;101:341–8. <http://dx.doi.org/10.1016/j.apenergy.2012.01.048>.
- [19] McCarty PL, Goltz MN, Hopkins GD, Dolan ME, Allan JP, Kawakami BT, et al. Full-scale evaluation of in situ cometabolic degradation of trichloroethylene in groundwater through toluene injection. *Environ Sci Technol* 1998;32(1):88–100. <http://dx.doi.org/10.1021/es970322b>.
- [20] Harbaugh AW. MODFLOW-2005, the U.S. geological survey modular ground-water model – the ground-water flow process. *U.S. Geol Surv Tech Methods* 2005;6-A16.
- [21] Luo J, Kitanidis PK. Fluid residence times within a recirculation zone created by an extraction–injection well pair. *J Hydrol* 2004;295(1–4):149–62. <http://dx.doi.org/10.1016/j.jhydrol.2004.03.006>.
- [22] Dungey JW. Interplanetary magnetic field and the auroral zones. *Phys Rev Lett* 1961;6:47–8. <http://dx.doi.org/10.1103/PhysRevLett.6.47>.
- [23] Cassak PA. Inside the black box: Magnetic reconnection and the magnetospheric multiscale mission. *Space Weather* 2016;14(3):186–97. <http://dx.doi.org/10.1002/2015SW001313>.
- [24] Birn J, Nakamura R, Panov EV, Hesse M. Bursty bulk flows and dipolarization in MHD simulations of magnetotail reconnection. *J Geophys Res Space Phys* 2011;116(A1). <http://dx.doi.org/10.1029/2010JA016083>.
- [25] Angelopoulos V, Artemyev A, Phan TD, Miyashita Y. Near-earth magnetotail reconnection powers space storms. *Nat Phys* 2020;16(3):317–21. <http://dx.doi.org/10.1038/s41567-019-0749-4>.
- [26] Glocer A, Dorelli J, Toth G, Komar CM, Cassak PA. Separator reconnection at the magnetopause for predominantly northward and southward IMF: Techniques and results. *J Geophys Res Space Phys* 2016;121(1):140–56. <http://dx.doi.org/10.1002/2015JA021417>.
- [27] Tóth G, Sokolov IV, Gombosi TI, Chesney DR, Clauer CR, Zeeuw DLD, et al. Space weather modeling framework: A new tool for the space science community. *J Geophys Res Space Phys* 2005;110(A12). <http://dx.doi.org/10.1029/2005JA011126>.
- [28] Morley SK, Welling DT, Woodroffe JR. Perturbed input ensemble modeling with the space weather modeling framework. *Space Weather* 2018;16(9):1330–47. <http://dx.doi.org/10.1029/2018SW002000>.
- [29] Tóth G, van der Holst B, Sokolov IV, De Zeeuw DL, Gombosi TI, Fang F, et al. Adaptive numerical algorithms in space weather modeling. *J Comput Phys* 2012;231(3):870–903. <http://dx.doi.org/10.1016/j.jcp.2011.02.006>, Special Issue: Computational Plasma Physics.
- [30] Haiducek JD, Welling DT, Ganushkina NY, Morley SK, Ozturk DS. SWMF Global magnetosphere simulations of January 2005: Geomagnetic indices and cross-polar cap potential. *Space Weather* 2017;15(12):1567–87. <http://dx.doi.org/10.1002/2017SW001695>.
- [31] Loewe CA, Pröls GW. Classification and mean behavior of magnetic storms. *J Geophys Res Space Phys* 1997;102(A7):14209–13. <http://dx.doi.org/10.1029/96JA04020>.
- [32] Zhang J, Dere KP, Howard RA, Bothmer V. Identification of solar sources of major geomagnetic storms between 1996 and 2000. *Astrophys J* 2003;582(1):520–33. <http://dx.doi.org/10.1086/344611>.
- [33] Lockwood M, Morley SK. A numerical model of the ionospheric signatures of time-varying magnetic reconnection: I. ionospheric convection. *Ann Geophys* 2004;22(1):73–91. <http://dx.doi.org/10.5194/angeo-22-73-2004>.
- [34] Ahrens J, Geveci B, Law C. *Paraview: An end-user tool for large data visualization*. In: *The visualization handbook*, Vol. 717. Elsevier München; 2005.
- [35] Childs H, Brugger E, Whitlock B, Meredith J, Ahern S, Pugmire D, et al. *Visit: An end-user tool for visualizing and analyzing very large data*. In: *High performance visualization—enabling extreme-scale scientific insight*. 2012, p. 357–72.
- [36] Bresciani E, Kang PK, Lee S. Theoretical analysis of groundwater flow patterns near stagnation points. *Water Resour Res* 2019;55(2):1624–50. <http://dx.doi.org/10.1029/2018wr023508>.
- [37] Tóth J. A theoretical analysis of groundwater flow in small drainage basins. *J Geophys Res* 1963;68(16):4795–812. <http://dx.doi.org/10.1029/JZ068i016p04795>.
- [38] Winter TC. *Numerical simulation analysis of the interaction of lakes and ground water*. In: *USGS Professional Paper*, Vol. 1001. U.S. Govt. Print. Off.; 1976, p. 1–45.

- [39] Bakker M, Strack ODL. Capture zone delineation in two-dimensional groundwater flow models. *Water Resour Res* 1996;32(5):1309–15. <http://dx.doi.org/10.1029/96wr00198>.
- [40] Cardenas MB, Jiang X-W. Groundwater flow, transport, and residence times through topography-driven basins with exponentially decreasing permeability and porosity. *Water Resour Res* 2010;46(11):W11538. <http://dx.doi.org/10.1029/2010wr009370>.
- [41] Bresciani E, Gleeson T, Goderniaux P, de Dreuzy JR, Werner AD, Wörman A, et al. Groundwater flow systems theory: Research challenges beyond the specified-head top boundary condition. *Hydrogeol J* 2016;24(5):1087–90. <http://dx.doi.org/10.1007/s10040-016-1397-8>.
- [42] Wang J-Z, Wörman A, Bresciani E, Wan L, Wang X-S, Jiang X-W. On the use of late-time peaks of residence time distributions for the characterization of hierarchically nested groundwater flow systems. *J Hydrol* 2016;543, Part:47–58. <http://dx.doi.org/10.1016/j.jhydrol.2016.04.034>.
- [43] Wang X-S, Wan L, Jiang X-W, Li H, Zhou Y, Wang J, et al. Identifying three-dimensional nested groundwater flow systems in a Tóthian basin. *Adv Water Resour* 2017;108:139–56. <http://dx.doi.org/10.1016/j.advwatres.2017.07.016>.